Comparison of gauge-model predictions at high Q^2: pp, $\bar{p}p$, and e^+e^- interactions

Thomas G. Rizzo
Department of Physics, Brookhaven National Laboratory, Upton, New York 11973
(Received 17 October 1979)

We compare the predictions of the $SU_L(2)\times U(1)$ and $SU_L(2)\times SU_R(2)\times U(1)$ gauge models for various pp, $\bar{p}p$, and e^+e^- processes at high Q^2. First, we calculate the masses, total widths, and branching ratios for the various neutral (Z°) gauge bosons in both models to show their parameter dependence. We then calculate their production cross sections for pp, $\bar{p}p$, and e^+e^- interactions. Further, we consider the forward-backward asymmetry and the polarization effects in e^+e^- annihilation for both models. We find that the best and perhaps the only way to distinguish the two models is to search for a second Z° boson in leptonic and hadronic reactions. The detection of such a particle may be possible with the next generation of accelerators.

I. INTRODUCTION

Since the recent model-independent analyses of the neutrino neutral-current data by several authors[1] and the results of Novosibirsk,[2] Berkeley,[3] and SLAC[4] experiments on the electron neutral current, the $SU_L(2)\times U(1)$ gauge model of Weinberg and Salam (WS)[5] seems stronger than ever. As is well known, however, it is possible that the correct weak-electromagnetic gauge group G_{wk} is larger than $SU_L(2)\times U(1)$ but contains it as a subgroup $G_{wk}\subset SU_L(2)\times U(1)$; under these conditions the low-energy phenomenology can be almost identical to the WS model.[5]

A particular example of this kind is the model by Sidhu[6] based on $SU_L(2)\times SU_R(2)\times U(1)$; as was shown in a series of papers[6,7] the low-energy predictions of this model compare as favorably to the data as do those of the standard WS model. It was also shown[7] that the high-energy deep-inelastic reactions $\overset{(-)}{\nu}p\to\overset{(-)}{\nu}X$ cannot be used to distinguish the two models even for ν energies of 1–10 TeV [the range to be explored by the deep underwater muon and neutrino detector (DUMAND)[8]]. Although a measurement of various weak asymmetries in $e^\pm p$ reactions could be used to discriminate the two models, the required Q^2 region ($Q^2>10^3$ GeV$^2/c^2$) awaits the construction of an ep collider.[9]

In this paper we would like to examine some of the predictions of the two models for e^+e^- as well as pp and $\bar{p}p$ reactions which can be studied at PEP, PETRA, ISABELLE,[18] LEP,[19] and the CERN $\bar{p}p$ collider.

In Sec. II, we give a brief review of the parameters of the left-right-symmetric theory; Sec. III contains a comparison of the predictions of the two models for forward-backward asymmetry, polarization effects, and the total cross section for e^+e^- interactions.

In Sec. IV, we analyze the properties of the neutral gauge bosons in both models over a range of parameters—mass, total widths, and branching ratios. Section V contains estimates of the production rates of the various neutral gauge bosons relevant for e^+e^-, pp, and $\bar{p}p$ reactions. Our conclusions can be found in Sec. VI.

II. REVIEW OF $SU_L(2)\times SU_R(2)\times U(1)$

In this section we would like to give a brief review of the parameters and couplings of the left-right-symmetric $SU_L(2)\times SU_R(2)\times U(1)$ gauge theory.[6,7] A full description of the model can be found in the references. If the neutral-current interaction is written as

$$\mathcal{L}_{\rm int}^{\rm NC}=-iJ_\mu^1 Z^{1\mu}-iJ_\mu^2 Z^{2\mu}\,, \tag{2.1}$$

then

$$\left.\begin{matrix}J_\mu^1\\ J_\mu^2\end{matrix}\right\}=\sum_i \psi_i\gamma_\mu\left[\frac{e}{2\sin\theta}\left\{\begin{matrix}\cos\phi\\ -\sin\phi\end{matrix}\right\}(T_{3L}^i+T_{3R}^i)\gamma_5+\frac{e}{\sin 2\theta}\left\{\begin{matrix}\sin\phi\\ \cos\phi\end{matrix}\right\}[(\cos^2\theta)(T_{3L}^i+T_{3R}^i)-2(\sin^2\theta)Y^i]\right]\psi_i\,, \tag{2.2}$$

where $T_{3L(R)}$ is the third component of left- (right-) handed weak isospin and Y is the weak hypercharge, such that the fermion charge is simply

$$Q^i=T_{3L}^i+T_{3R}^i+Y^i\,,$$

the index i runs over all fermion types. We have

$$T_{3L}^e=T_{3R}^e=T_{3L}^d=T_{3R}^d=-\tfrac{1}{2}\,,$$

$$T_{3L}^u=T_{3R}^u=T_{3L}^\nu=\tfrac{1}{2}\,,$$

$$Y^u = Y^d = \tfrac{1}{6}, \quad Y^e = -\tfrac{1}{2}, \quad \text{etc.}$$

Here, the role of $\sin\theta$ parallels that of $\sin\theta_W$ in the WS model; however, we find

$$\begin{pmatrix}\cos\phi\\ \sin\phi\end{pmatrix} = \begin{pmatrix} C \\ (\epsilon-1)\zeta\end{pmatrix} [(1-\epsilon)^2\zeta^2 + C^2]^{-1/2}, \quad (2.3)$$

with

$$C = -\tfrac{1}{2}(1-\epsilon)\sin^2\theta\sec\theta + \epsilon\cos\theta - \{[\tfrac{1}{2}(1-\epsilon)\sin^2\theta\sec\theta - \epsilon\cos\theta]^2 + (1-\epsilon)^2\zeta^2\}^{1/2}. \quad (2.4)$$

The parameters ϵ and ζ express certain ratios of vacuum expectation values and are constrained to lie in the ranges

$$0 \le \epsilon \le 1, \qquad -1 \le \zeta \le 1. \quad (2.5)$$

Along with $\sin^2\theta$ these are the three parameters of this model; the present neutral-current data seem to constrain these parameters to certain regions[6,7]:

$$\epsilon \approx 0, \qquad \zeta \ge 0.65, \qquad 0.4 \le \sin^2\theta \le 0.5. \quad (2.6)$$

The analysis that follows will assume the above range of the various parameters. We note that in the limit

$$\epsilon \to 0, \qquad \zeta \to 1, \qquad \sin^2\theta \to 2\sin^2\theta_W, \quad (2.7)$$

we recover exactly the currents of the WS model. In terms of these parameters the gauge-boson masses are (assuming $M_{W_R} \gg M_{W_L}$)

$$M_{W_L^\pm}^2 = \frac{2\pi\alpha}{\sqrt{2}G_F}\frac{1}{\sin^2\theta} \quad (2.8)$$

and

$$\begin{pmatrix} M_{Z_1}^2 \\ M_{Z_2}^2\end{pmatrix} = \frac{M_{W_L^\pm}^2}{2[1-(1-\epsilon)\phi]}\{(1-\epsilon)\sec^2\theta + (1+\epsilon) \mp [(1+\epsilon) - (1-\epsilon)\sec^2\theta] + 4(1-\epsilon)^2\zeta^2\sec^2\theta\}^{1/2}.$$

In the limit (2.7), $M_{Z_1} \to (M_Z)_{WS}$, $M_{Z_2} \to \infty$, and $M_{W_L} \to (M_W)_{WS}$; we will not discuss the charged bosons further in our analysis since the right-handed boson W_R can be made arbitrarily heavy leaving the couplings of W_L identical with that found for the W of the WS model with the replacement $\sin^2\theta \to 2\sin^2\theta_W$.

III. NEUTRAL-CURRENT EFFECTS ON e^+e^- INTERACTIONS

We will now consider the various effects of parity-violating neutral currents on the reaction $e^+e^- \to \mu^+\mu^-$. (We follow the analysis given in Ref. 10.) Assuming μ-e universality we take our Lagrangian to be of the form

$$\mathcal{L} = \sum_{i=1}^{N}[\bar{e}\gamma_\mu(v_i + a_i\gamma_5)e + \mu\gamma_\mu(v_i + a_i\gamma_5)\mu]Z_i^\mu, \quad (3.1)$$

where we have assumed that there are N neutral gauge bosons. The differential cross section for $e^+e^- \to \mu^+\mu^-$ can now be written as (neglecting the μ mass)

$$\frac{d\sigma}{d\Omega} = \frac{\alpha^2}{4s}[A(1+\cos^2\theta) + 2B\cos\theta], \quad (3.2)$$

with

$$A = 1 + 2\sum_i\left(\frac{v_i}{e}\right)\frac{s}{s-M_i^2} + \sum_{i,i'}\frac{(v_i^2+a_i^2)(v_{i'}^2+a_{i'}^2)}{e^4}\left(\frac{s}{s-M_i^2}\right)\left(\frac{s}{s-M_{i'}^2}\right) \quad (3.3)$$

and

$$B = 2\sum_i\left(\frac{a_i}{e}\right)^2\frac{s}{s-M_i^2} + 4\sum_{i,i'}\frac{v_ia_i}{e^2}\frac{v_{i'}a_{i'}}{e^2}\left(\frac{s}{s-M_i^2}\right)\left(\frac{s}{s-M_{i'}^2}\right). \quad (3.4)$$

The forward-backward asymmetry is now defined as

$$A_{FB} = \frac{\int_0^1 d\cos\theta\, d\sigma - \int_{-1}^0 d\cos\theta\, d\sigma}{\int_{-1}^1 d\cos\theta\, d\sigma} = \tfrac{3}{4}B/A. \quad (3.5)$$

The total cross section is found to be

$$\sigma_{tot} = \frac{4\pi\alpha^2}{3s}A. \quad (3.6)$$

If the initial e^+e^- beams are unpolarized, the differential cross section as a function of the helicity of the final μ can be written as

$$\frac{d\sigma}{d\Omega} = \sigma_1 + h_\mu\sigma_2, \quad (3.7)$$

with

$$\sigma_1 \equiv \frac{1}{2}\frac{d\sigma}{d\Omega}, \quad (3.8)$$

which is given by Eq. (3.2). If we now define the average helicity as

$$H^\mu(\theta,s) = \sigma_2/\sigma_1, \quad (3.9)$$

we find

$$H^{\mu}(s,\cos\theta)=\frac{-2\Sigma}{A(1+\cos^2\theta)+2B\cos\theta}\times(1+\cos\theta)^2\,, \tag{3.10}$$

where

$$\Sigma=\sum_{l}\frac{a_l v_l}{e^2}\frac{s}{s-M_l^{\,2}}+\sum_{l,l'}\frac{a_l v_l(a_{l'}^{\,2}+v_{l'}^{\,2})}{e^4}\left(\frac{s}{s-M_l^{\,2}}\right)\left(\frac{s}{s-M_{l'}^{\,2}}\right). \tag{3.11}$$

We now define the forward helicity as

$$H_F^{\mu}=H^{\mu}(s,\cos\theta=1)=-\frac{4\Sigma}{A+B} \tag{3.12}$$

and the angular-averaged helicity by

$$\bar{H}_{\mu}=\frac{-2\Sigma\int_{-1}^{1}(1+\cos\theta)^2 d(\cos\theta)}{\int_{-1}^{1}d(\cos\theta)[A(1+\cos^2\theta)+2B\cos\theta]}=-2\Sigma/A\,. \tag{3.13}$$

In our analysis, the quantities of interest will then be $A_{\rm FB}$, A, H_F^{μ}, and $\bar{H}^{\mu}$. For the WS model and the $SU_L(2)\times SU_R(2)\times U(1)$ model the above expressions can easily be evaluated using the information of Sec. II. Let us first consider the region $\sqrt{s}\leq 50$ GeV/c which can be studied by PEP and PETRA in the near future.

Figures 1 and 2 show H_{FB}, H_F^{μ}, and $\bar{H}^{\mu}$ for the WS and two representative left-right-symmetric models for $\sqrt{s}\leq 50$ GeV/c; the two cases selected are somewhat extreme given the restricted range of parameters (2.6). (For the WS model we take $x_W=0.225$ in agreement with the neutral current and SLAC data.) As can easily be seen from Fig. 1, a measurement of $A_{\rm FB}$ at the 10% level would have difficulty differentiating the two models from the WS model. Figure 2, however, shows that the various predictions for the helicity parameters are much more distinct than those for $A_{\rm FB}$. A measurement of $\bar{H}^{\mu}$ and H_F^{μ} at the 10% level would constrain greatly the range of the parameters and rule out extreme cases. The clearest results are obtained for $\sqrt{s}\geq 30$ GeV/c.

It should be noted that a measurement of the total cross section will not necessarily give the value of A directly due to large radiative corrections and, hence, A is a poor parameter to use in comparing various models. On resonance, of course, A does become a good parameter since it essentially measures the total resonance width into $\mu^+\mu^-$.

Although a measurement at the 10% level can distinguish among the models we have chosen as examples, the parameters ξ, ϵ, and $\sin^2\theta$ can, of course, be chosen such that the WS model and the left-right-symmetric model with these parameters are indistinguishable even at the level of 1%. Measurements of the various asymmetries and cross sections presented here would only further constrain the parameters while ruling out a large class of models.

If larger e^+e^- machines were available (such as LEP) distinguishing among the various models would be much easier. Figure 3 shows the curves

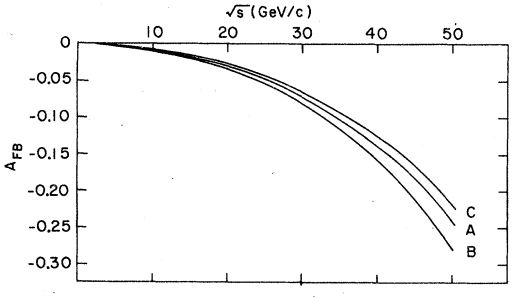

FIG. 1. A comparison of the prediction for $A_{\rm FB}$ for $\sqrt{s}\leq 50$ GeV/c; A: WS model with $x_W=0.225$; B: $\xi=0.7$, $\epsilon=0$, $\sin^2\theta=0.45$; C: $\xi=0.95$, $\epsilon=0.1$, $\sin^2\theta=0.40$.

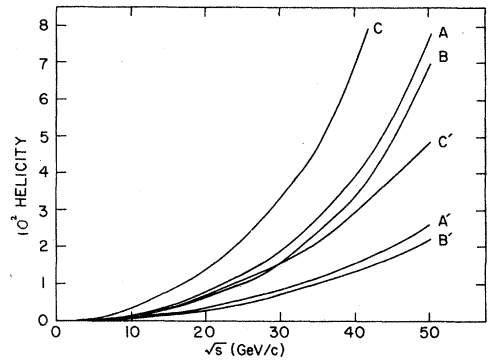

FIG. 2. A comparison of the predictions for H_F^{μ} (unprimed) and $\bar{H}^{\mu}$ (primed) for the same models presented in Fig. 1 with $\sqrt{s}\leq 50$ GeV/c.

Although a measurement at the 10% level can distinguish among the models we have chosen as examples, the parameters ξ, ϵ, and $\sin^2\theta$ can, of course, be chosen such that the WS model and the left-right-symmetric model with these parameters are indistinguishable even at the level of 1%. Measurements of the various asymmetries and cross sections presented here would only further constrain the parameters while ruling out a large class of models.

If larger e^+e^- machines were available (such as LEP) distinguishing among the various models would be much easier. Figure 3 shows the curves

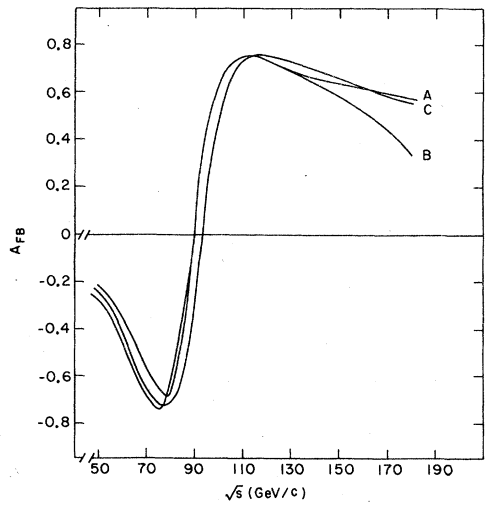

FIG. 3. Predictions for $A_{\rm FB}$ with $50\leq\sqrt{s}\leq 180$ GeV/c. The models are the same as those in Figs. 1 and 2.

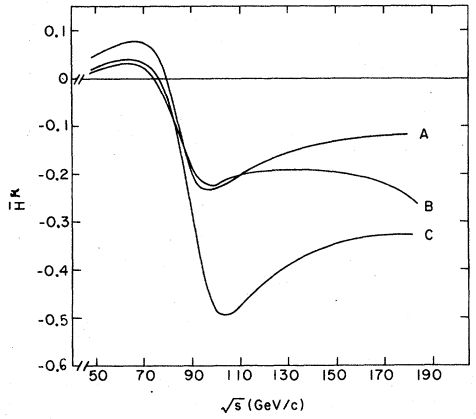

FIG. 4. Predictions for $\bar{H}^\mu$ with $50 \leq \sqrt{s} \leq 180$ GeV/c. The models are the same as those in Figs. 1–3.

of A_{FB} for the same models considered earlier; for $\sqrt{s} \geq 50$ GeV/c, as is easily seen, the three models chosen are clearly distinguishable at the 10% level throughout most of this center-of-mass energy range.

Figure 4 shows the plots of $\bar{H}^\mu$; again, the three models can easily be distinguished for $\sqrt{s} \geq 110$ GeV/c. For smaller $\sqrt{s}$ values models A and B can be distinguished at the 10% level. Similarly, Fig. 5 shows the plots of H_F^μ; we again see that the three models are easily distinguished.

We would again like to point out that the left-right-symmetric models we have chosen are only representative of a class of such models whose predictions at high Q^2 differ significantly from those of the WS model. The range of parameters is such that there are some models of the left-right-symmetric type which cannot be ruled out by high-Q^2 e^+e^- data even if it were known at the 1% level. However, a large class of models allowed by the low-energy data can be eliminated (or at least tested) by such measurements.

To study e^+e^- interactions further, we must know something about the various gauge bosons in the left-right-symmetric model and how they compare to their WS relatives.

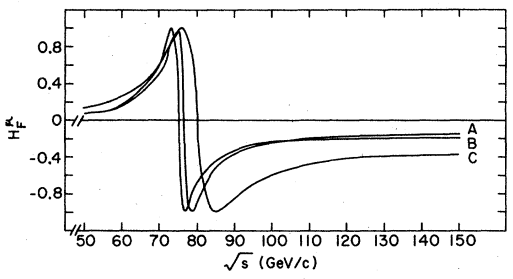

FIG. 5. Predictions for H_F^μ with $50 \leq \sqrt{s} \leq 180$ GeV/c. The models are the same as those in Figs. 1–4.

IV. GAUGE BOSONS IN LEFT-RIGHT-SYMMETRIC MODELS

We now turn our attention to the properties of the gauge bosons of the left-right-symmetric theory and ask how they compare to those of the standard WS model. Let us first examine the charged bosons in the theory; here, there are two different approaches possible depending on the symmetry-breaking scheme.[6,11] In both of these approaches, we have three Higgs fields of the form $\chi_L(\frac{1}{2},0,\frac{1}{2})$, $\chi_R(0,\frac{1}{2},\frac{1}{2})$, and $\phi(\frac{1}{2},\frac{1}{2},0)$ with vacuum expectation values (VEV's) [we take ϕ to be real]:

$$\langle\chi_L\rangle=\begin{bmatrix}0\\ \lambda_L\end{bmatrix}, \quad \langle\chi_R\rangle=\begin{bmatrix}0\\ \lambda_R\end{bmatrix}, \quad \phi=\begin{bmatrix}\kappa & 0\\ 0 & \kappa'\end{bmatrix}. \tag{4.1}$$

In the first approach these are the only Higgs fields[11]; the second approach includes two triplets $\delta_L(1,0,0)$ and $\delta_R(0,1,0)$ with VEV's

$$\langle\delta_L\rangle=0, \quad \langle\delta_R\rangle=\begin{bmatrix}0\\ \Lambda\\ 0\end{bmatrix}, \tag{4.2}$$

and $\Lambda \gg \kappa, \kappa', \lambda_L, \lambda_R$. In the latter case, for phenomenological purposes, we can treat the fields $W_{L,R}^+$ as mass eigenstates independent of ξ, ϵ, or $\sin^2\theta$. In the former case, the mass eigenstates are, in general, some mixture of W_L^+ and W_R^+ (which we call W_1^+ and W_2^+) and no longer couple to currents of a given chirality.

If we write

$$\vec{J}\cdot\vec{W}\equiv J_L W_L + J_R W_R \tag{4.3}$$

in terms of mass eigenstates through the rotation

$$\begin{bmatrix}W_1\\ W_2\end{bmatrix}=\begin{bmatrix}c & -s\\ s & c\end{bmatrix}\begin{bmatrix}W_L\\ W_R\end{bmatrix} U \begin{bmatrix}W_L\\ W_R\end{bmatrix}, \tag{4.4}$$

the effective charged-current Hamiltonian is

$$\mathcal{H}_{CC}^{\text{eff}}=\tfrac{1}{8}g^2\left[\frac{J_1^\dagger J_1}{M_{W_1}^2}+\frac{J_2^\dagger J_2}{M_{W_2}^2}\right], \tag{4.5}$$

with

$$\begin{bmatrix}J_1\\ J_2\end{bmatrix}=U\begin{bmatrix}J_L\\ J_R\end{bmatrix}. \tag{4.6}$$

Here $c=\cos\theta$, $s=\sin\theta$. In terms of chiral currents, $\mathcal{H}_{CC}^{\text{eff}}$ takes the form

$$\mathcal{H}_{CC}^{\text{eff}}=\frac{g^2}{8}\left[\left(\frac{c^2}{M_{W_1}^2}+\frac{s^2}{M_{W_2}^2}\right)J_L^\dagger J_L+\left(\frac{s^2}{M_{W_1}^2}+\frac{c^2}{M_{W_2}^2}\right)J_R^\dagger J_R + \left(\frac{1}{M_{W_2}^2}-\frac{1}{M_{W_1}^2}\right)cs(J_L^\dagger J_R+J_R^\dagger J_L)\right]. \tag{4.7}$$

Since the usual charge currents are consistent

with being left-handed, the coefficients of $J_R^\dagger J_R$ and $(J_L^\dagger J_R + J_R^\dagger J_L)$ must be small by comparison to the coefficient of $J_L^\dagger J_L$; improved data on the chiral structure of charged currents in μ decay would greatly reduce the allowed range of ϵ and ζ.

For this case we find

$$M_{W_{1,2}}{}^2 = \tfrac{1}{2} g^2 \lambda_R{}^2 \{\tfrac{1}{2}(1+\lambda+2k) \pm \tfrac{1}{2}[(1-\lambda)^2 + 4k^2]^{1/2}\}, \tag{4.8}$$

where

$$\lambda \equiv \lambda_L{}^2/\lambda_R{}^2 = \frac{1-\zeta}{1+\zeta}, \qquad k \equiv \frac{\kappa^2+\kappa'^2}{\lambda_R{}^2} = \frac{\epsilon}{(1-\epsilon)(1+\zeta)}. \tag{4.9}$$

We note that as $\epsilon \to 0$ (independent of ζ), we find $W_{1,2} = W_{L,R}$ giving

$$M_{W_{1,2}}{}^2 = \tfrac{1}{2} g^2 \lambda_{L,R}{}^2, \quad \theta = 0. \tag{4.10}$$

Since the range of parameters (2.6) is already consistent with the present charged-current data further experiment is needed to examine this option further.

Since the relation between the masses of the two charged W's is unknown at this time (the lighter of the two couples essentially to left-handed currents and has mass and decay properties very similar to the WS gauge boson) we will not consider the charged W's further in our discussion. For our purposes we will assume that $M_W{}^2$ is defined via

$$G_F/\sqrt{2} = g^2/8M_1{}^2. \tag{4.11}$$

We now turn our attention to the neutral gauge bosons. The masses of these particles are independent of the choice of the two symmetry-breaking schemes discussed above and are given by Eq. (2.9). The mass of the lighter Z boson is comparable to that of the WS Z boson and is quite insensitive to the values of ϵ or ζ. Figures 6 and 7 show the parameter dependence of the two Z boson masses in the left-right-symmetric model.

The mass of the lighter Z (Z_1) is in the region 85–95 GeV over a wide range of ζ, ϵ, and $\sin^2\theta$ values; note that the WS prediction is in the middle of the range of Z_1 mass values. Note also that the sensitivity of the Z_1 mass to variations in ζ, ϵ, or $\sin^2\theta$ is just about identical. For the heavier Z (Z_2) the mass is very sensitive to variations in ζ and ϵ although not so sensitive to variations in $\sin^2\theta$. Note that for fixed ζ and $\sin^2\theta$ an increase in the value of ϵ reduces the Z_2 mass, substantially so for large ζ values. This will greatly effect the total width of the particle and increase the chance of its observation.

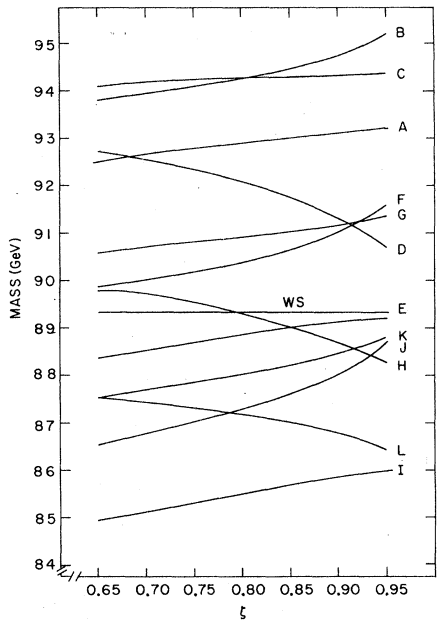

FIG. 6. The mass of the lighter Z boson for several models; A: $\epsilon=0$, $\sin^2\theta=0.40$; B: $\epsilon=0.05$, $\sin^2\theta=0.4$; C: $\epsilon=0.1$, $\sin^2\theta=0.4$; D: $\epsilon=0.2$, $\sin^2\theta=0.4$; E: $\epsilon=0$, $\sin^2\theta=0.45$; F: $\epsilon=0.05$, $\sin^2\theta=0.45$; G: $\epsilon=0.1$, $\sin^2\theta=0.45$; H: $\epsilon=0.2$, $\sin^2\theta=0.45$; I: $\epsilon=0$, $\sin^2\theta=0.5$; J: $\epsilon=0.05$, $\sin^2\theta=0.5$; K: $\epsilon=0.1$, $\sin^2\theta=0.5$; L: $\epsilon=0.2$, $\sin^2\theta=0.5$; WS is the standard-model prediction.

We now turn to the decay modes of Z_1 and Z_2; Figs. 8 and 9 show the parameter dependence of the total widths of Z_1 and Z_2, respectively. Note

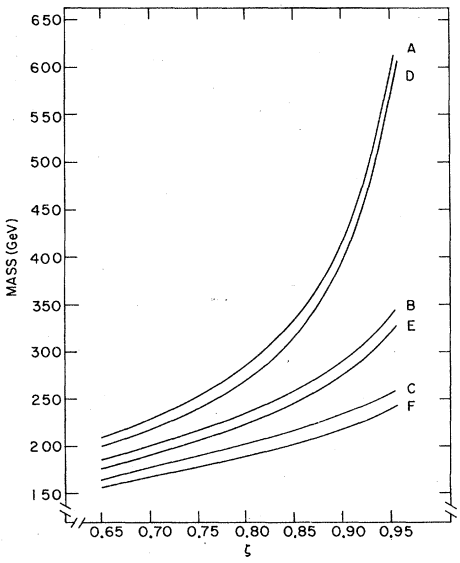

FIG. 7. Mass of the heavy Z (Z_2) in $SU_L(2)\times SU_R(2)\times U(1)$; A: $\epsilon=0$, $\sin^2\theta=0.4$; B: $\epsilon=0.1$, $\sin^2\theta=0.4$; C: $\epsilon=0.2$, $\sin^2\theta=0.4$; D: $\epsilon=0$, $\sin^2\theta=0.5$; E: $\epsilon=0.1$, $\sin^2\theta=0.5$; F: $\epsilon=0.2$, $\sin^2\theta=0.5$.

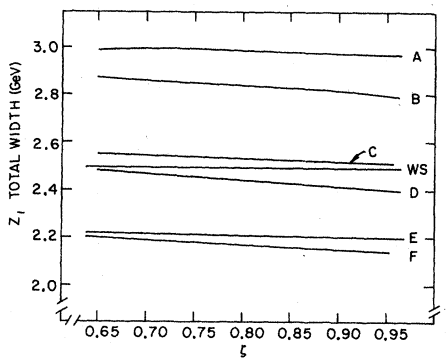

FIG. 8. Total width of the Z_1 for various model parameters; A: $\epsilon=0$, $\sin^2\theta=0.4$; B: $\epsilon=0.2$, $\sin^2\theta=0.4$; C: $\epsilon=0$, $\sin^2\theta=0.45$; D: $\epsilon=0.2$, $\sin^2\theta=0.45$; E: $\epsilon=0$, $\sin^2\theta=0.5$; F: $\epsilon=0.2$, $\sin^2\theta=0.5$; WS is the standard Weinberg-Salam prediction.

that the total width of Z_1 is quite insensitive to the value of ϵ or ζ as is only somewhat sensitive to the value of $\sin^2\theta$ over the range examined; the Z_2 total width, however, is quite sensitive to the values of ϵ, ζ, and $\sin^2\theta$ since its mass is strongly dependent on these parameters. We remind the reader that the decay rate for Z (Z_1 or Z_2) $\to \bar{f}f$ (f is some fermion) is given by

$$\Gamma_f=(3)\frac{M_Z}{12\pi}\left(1-\frac{4m^2}{M_Z{}^2}\right)^{1/2} \times\left[\left(1+\frac{2m^2}{M_Z{}^2}\right)g_V{}^2+\left(1-\frac{4m^2}{M_Z{}^2}\right)g_A{}^2\right], \tag{4.12}$$

where g_V, g_A are defined through [via Eq. (2.2)]

$$\mathcal{L}^{\text{eff}}=-i\bar{f}\gamma_\mu(g_V-g_A\gamma_5)fZ^\mu \tag{4.13}$$

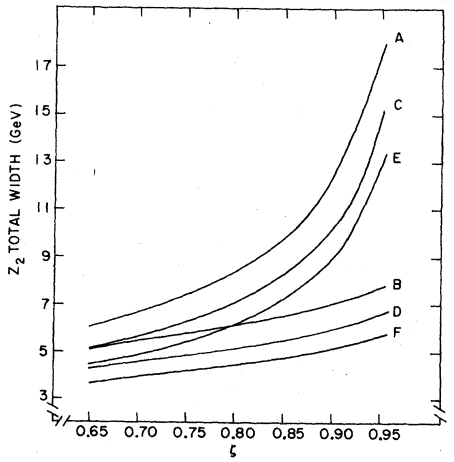

FIG. 9. Total width of the Z_2 for various model parameters. The models chosen are the same as those appearing in Fig. 8.

and m is the mass of the fermion f. (The color factor of 3 in the above expression arises if f is a quark.) Note that since $\Gamma\sim m_Z$ the total width has almost the same parameter dependence as does the particle mass. In calculating the various widths we have used the following constituent quark masses[12]:

$$\begin{aligned} m_u\simeq m_d&=0.34\text{ GeV},\\ m_s&=0.54\text{ GeV},\\ m_c&=1.66\text{ GeV},\\ m_b&=5.0\text{ GeV},\\ m_t&=15.0\text{ GeV}. \end{aligned} \tag{4.14}$$

We now turn our attention to the various branching ratios, the most important of which is for $Z\to\mu^+\mu^-$ since the search for Z's in pp or $\bar{p}p$ will be in the channel $pp(\bar{p}p)\to\mu^+\mu^-x$. Figure 10 shows the parameter dependence of the branching ratio for Z (Z_1 and Z_2) $\to\mu^+\mu^-$; for Z_1 the ζ dependence is very weak and only somewhat stronger in the case of Z_2. The branching ratio in both cases is quite sensitive to ϵ and $\sin^2\theta$.

We conclude this section with our results on the branching ratio for $Z_{1,2}\to$ hadrons and the ratio

$$R_{1,2}=\frac{Z_{1,2}\to d\bar{d}}{Z_{1,2}\to u\bar{u}}. \tag{4.15}$$

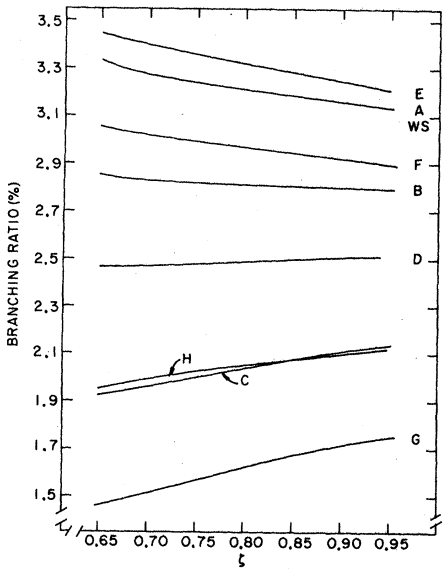

FIG. 10. Branching ratio for $Z\to\mu^+\mu^-$ (for both Z_1 and Z_2) for various model parameters: A: $\epsilon=0$, $\sin^2\theta=0.4$ (Z_1); B: $\epsilon=0.2$, $\sin^2\theta=0.4$ (Z_1); C: $\epsilon=0$, $\sin^2\theta=0.4$ (Z_2); D: $\epsilon=0.2$, $\sin^2\theta=0.4$ (Z_2); E: $\epsilon=0$, $\sin^2\theta=0.5$ (Z_1); F: $\epsilon=0.2$, $\sin^2\theta=0.5$ (Z_1); G: $\epsilon=0$, $\sin^2\theta=0.5$ (Z_2); H: $\epsilon=0.2$, $\sin^2\theta=0.5$ (Z_2); WS is the prediction of the standard model.

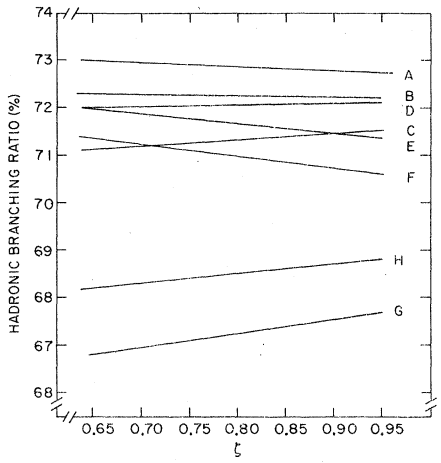

FIG. 11. Total hadronic branching ratio for both Z_1 and Z_2 for various model parameters. The models chosen are the same as those appearing in Fig. 10.

Figure 11 shows our results for the branching ratio $Z_{1,2} \to$ hadrons/$Z_{1,2} \to$ all for various values of the parameters. Note that the numerical value in both cases is roughly constant at ~70% quite independent of the values of ϵ, ζ, or $\sin^2\theta$. (The WS-model prediction for the hadronic branching ratio is 72.1% for $x_W = 0.225$.) Figure 12 shows the plots for the ratios $R_{1,2}$ defined in Eq. (4.15); the R ratio for the WS model is 1.29 for $x_W = 0.225$. The ratios $R_{1,2}$ are quite insensitive to the value of ζ; R_1 is

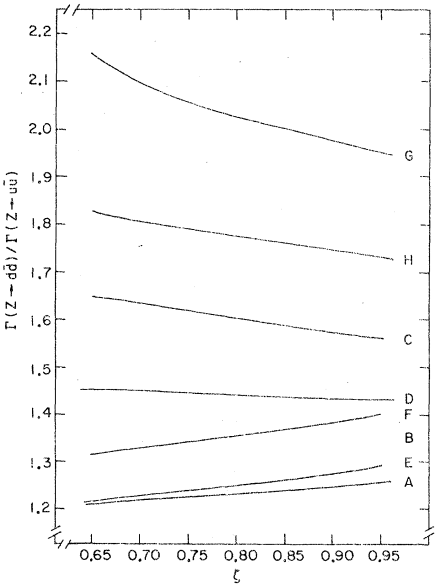

FIG. 12. The ratio of widths $\Gamma(Z \to d\bar{d})/\Gamma(Z \to u\bar{u})$ for both Z_1 and Z_2 for various model parameters. The models chosen are the same as those appearing in Figs. 10 and 11.

insensitive to $\sin^2\theta$ and only mildly sensitive to ϵ. R_2 is quite sensitive to changes in either ϵ or $\sin^2\theta$.

Using the various branching ratios we have presented we can easily obtain the branching ratios for Z decay into any $\bar{f}f$ pair in the limit that we can neglect the fermion masses (the only questionable case is for $Z_1 \to \bar{t}t$) which is a very good approximation. A little algebra shows that:

$$B(Z \to \nu\bar{\nu}) = \frac{T - H - 3l}{3}\,,$$
$$B(Z \to u\bar{u}) = H/3(1+R)\,, \tag{4.16}$$
$$B(Z \to d\bar{d}) = HR/3(1+R)\,,$$

where

$$T = \Gamma(Z \to \text{all})\,,$$
$$H = \Gamma(Z \to \text{hadrons})\,, \tag{4.17}$$
$$l = \Gamma(Z \to l^+l^-)\,.$$

V. PRODUCTION OF Z_1 AND Z_2 IN pp, $\bar{p}p$, AND e^+e^- INTERACTIONS

In this section we will discuss the production rates of Z_1, Z_2 in pp, $\bar{p}p$, and e^+e^- interactions and compare them with those for the single Z of the WS model. We will discuss the pp and $\bar{p}p$ production mechanism first.

In the standard Drell-Yan picture,[13] Z production in pp or $\bar{p}p$ collisions proceeds through $\bar{q}q$ annihilation in a manner completely parallel to dimuon production via a single, massive photon [we will neglect any quantum-chromodynamics (QCD) corrections in our discussion below]. The cross section for $a + b \to Z + X$ can be written as[14,15]

$$\frac{d\sigma}{dx_F} = \frac{2\pi}{3M_Z{}^2}\frac{x_a x_b}{(x_F{}^2 + 4\tau)^{1/2}} \times \sum_i (g_L^{i2} + g_R^{i2})[q_a^i(x_a)\bar{q}_b^i(x_b) + \bar{q}_a^i(x_a)q_b^i(x_b)]\,, \tag{5.1}$$

where i labels the flavor of the quark with chiral couplings $g^i_{L,R}$ to Z. Here $q_a^i(x_a)$ is the quark distribution function for a quark of flavor i inside hadron a evaluated at x_a, etc. We have defined

$$\tau = M_Z{}^2/s\,,$$
$$x_{a,b} = \tfrac{1}{2}[(x_F{}^2 + 4\tau)^{1/2} \pm x_F]\,, \tag{5.2}$$

with x_F being the standard Feynman variable and s is the square of the center-of-mass energy. The couplings $g^i_{L,R}$ are well known for the WS model and can be read off directly from Eq. (2.2) for the left-right-symmetric model.

Since we consider only pp and $\bar{p}p$ production of Z's we need only the quark distribution functions

of the proton; we take for purposes of demonstration the Field-Feynman distributions[16] with charm included (we neglect the contents of quarks heavier than c in the proton):

$$\begin{aligned} xu(x) &= 1.14(1-x)^3 , \\ xd(x) &= 2.9(1-x)^4 , \\ x\bar{u}(x) &= 0.17(1-x)^{10} , \\ x\bar{d}(x) &= 0.17(1-x)^7 , \\ xs(x) &= x\bar{s}(x) = 0.1(1-x)^{10} , \\ xc(x) &= x\bar{c}(x) = 0.03(1-x)^{10} . \end{aligned} \tag{5.3}$$

To get the total cross section, σ_{tot}, we merely integrate Eq. (4.1) over the range (for any fixed value of τ):

$$-(1-\tau) \leq x_F \leq 1-\tau . \tag{5.4}$$

In our calculations we have assumed that the parton distributions scale which should not be too bad an approximation for the pp case, especially for small τ, since it is a valence×sea process (QCD increases the sea while decreasing the valence distribution with increasing $M_Z{}^2$). The effect of QCD corrections for the heavier Z will be much greater since for large $\sqrt{\tau}$ (large $x_a x_b$) both sea and valence distributions are decreased. We thus expect our results for Z_2 to be upper limits. For light Z's, since we are making a comparison of production rates we are not too concerned about these effects; in particular, since the detection of a Z depends crucially on the branching ratio into $\mu^+\mu^-$ we will compare only production cross section×branching ratios (σB) for the various models. Figure 13 contains the predictions for σB for the single Z boson of the WS model with $x_W = 0.225$ for both pp and $\bar{p}p$ reactions; the general shape of the curves for σB is well represented by this case.

Since we are mainly interested in producing Z bosons at ISABELLE (pp, $\sqrt{s} = 800$ GeV/c) or the CERN $\bar{p}p$ collider ($p\bar{p}$, $\sqrt{s} = 540$ GeV/c) we will only evaluate σB for the various models at these $\sqrt{s}$ values. For example, at ISABELLE the WS model Z has a σB of $\sim 5.1 \times 10^{-35}$ leading to an event rate of roughly $\sim 4.4 \times 10^3$ events/day if a luminosity of 10^{33} cm^{-2} sec^{-1} is assumed. On the other hand, at the CERN $\bar{p}p$ collider, we find a σB of $\sim 3.0 \times 10^{-34}$ which yields an event rate of $\sim 2.6 \times 10^1$/day assuming a luminosity of 10^{30}. It should be remembered that these counting rates are an optimistic overestimate but clearly show that counting rates at ISABELLE are more than two orders of magnitude larger than at the CERN $\bar{p}p$ collider.

Our results, Figs. 14 and 15, show the values of σB for the various models relevant for ISABELLE or CERN $\bar{p}p$ collider. Figure 14 shows a comparison of Z_1 production rates (σB) for various models at both ISABELLE or CERN; the ζ and $\sin^2\theta$ dependence is not very strong. We have also examined the ϵ dependence and found it to be somewhat stronger. This rather weak dependence results

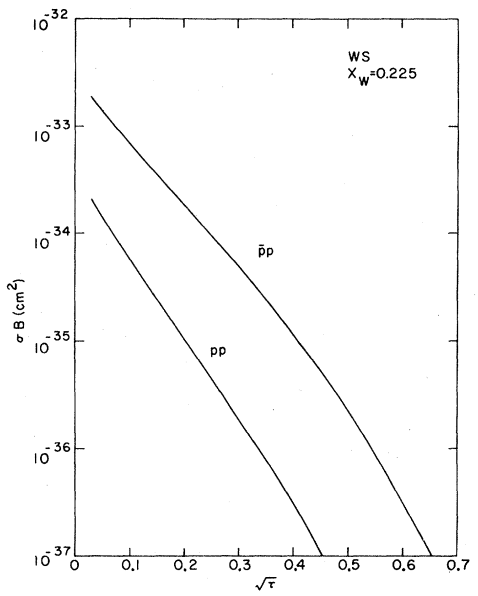

FIG. 13. σB for Z production in the channels pp, $\bar{p}p \to \mu^+\mu^- X$ in the WS model ($x_W = 0.225$) as a function of $\sqrt{\tau}$.

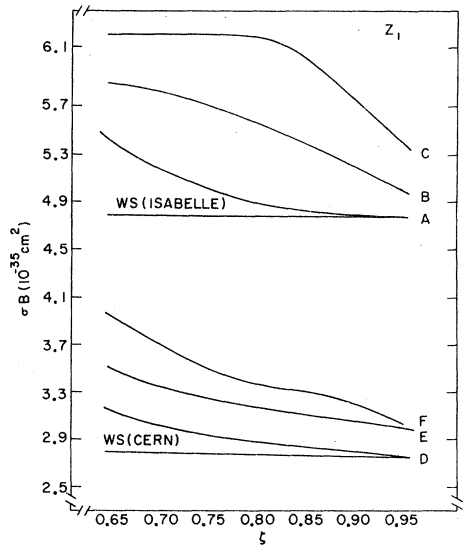

FIG. 14. σB for Z_1 production for various models ($\epsilon = 0$) at ISABELLE ($\sqrt{s} = 800$ GeV/c) and CERN ($\sqrt{s} = 540$ GeV/c) compared to the WS predictions. A: $\sin^2\theta = 0.4$ (ISABELLE); B: $\sin^2\theta = 0.45$ (ISABELLE); C: $\sin^2\theta = 0.5$ (ISABELLE); D: $\sin^2\theta = 0.4$ (CERN); E: $\sin^2\theta = 0.45$ (CERN); F: $\sin^2\theta = 0.5$ (CERN).

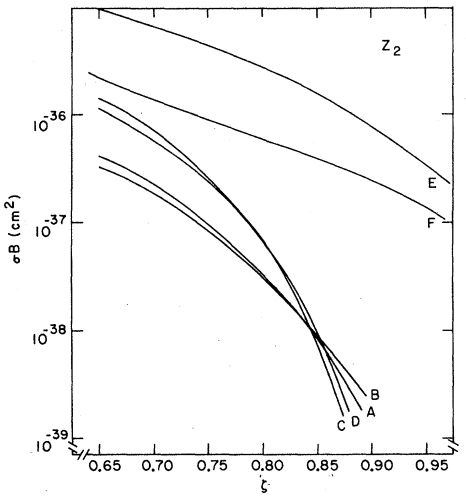

FIG. 15. σB for Z_2 production for several models at ISABELLE ($\sqrt{s}=800$ GeV/c) and CERN ($\sqrt{s}=540$ GeV/c). A: $\epsilon=0$, $\sin^2\theta=0.4$ (ISABELLE); B: $\epsilon=0$, $\sin^2\theta=0.5$ (ISABELLE); C: $\epsilon=0$, $\sin^2\theta=0.4$ (CERN); D: $\epsilon=0$, $\sin^2\theta=0.5$ (CERN); E: $\epsilon=0.2$, $\sin^2\theta=0.4$ (CERN); F: $\epsilon=0.2$, $\sin^2\theta=0.4$ (ISABELLE).

from the weak dependence of the fermion couplings to and mass of the Z_1 gauge boson to the parameters ζ, ϵ, and $\sin^2\theta$.

Figure 15 shows a comparison of Z_2 production rates (σB) at both CERN and ISABELLE, for various models. Here the rates are highly parameter dependent because of the sensitivity of the Z_2 mass. In this case, because of QCD corrections, we can regard these values of σB as upper limits at best.

We now ask if it is likely that a Z_2 could be produced at ISABELLE or CERN with any appreciable counting rate in the $pp(\bar{p}p)\to\mu^+\mu^- x$ channel. As an example, we consider a model with $\epsilon=0$, $\zeta=0.85$, $\sin^2\theta=0.45$ for which $\sqrt{\tau}\simeq 0.41$ at ISABELLE and $\simeq 0.61$ at CERN for Z_2 production. Using the above luminosities we find a counting rate ~1 event/day at ISABELLE and ~10^{-3} event/day at CERN; obviously such a particle could not be seen at the CERN $\bar{p}p$ collider. The counting rate at ISABELLE is small and is further decreased by QCD corrections. Although the electromagnetic background is smaller (by ~10^2), a thorough knowledge of the strong background, i.e., μ's from quark decays, etc., is necessary. We believe that the outlook for this particular model is not optimistic although, with a thorough understanding of the background, detection of a heavy Z may be possible. The detection of a heavy Z would be positive proof that the weak-interaction gauge group needs to be extended beyond the standard SU(2)×U(1) WS model structure.

We now must examine the production properties of Z bosons in e^+e^- annihilation at LEP; in e^+e^- reactions we can search for Z's in either the leptonic (e^+e^- or $\mu^+\mu^-$) or hadronic channels (by measuring R). The resonance cross section in the channel $Z\to f\bar{f}$ is given by[10]

$$\frac{\sigma(e^+e^-\to f\bar{f})}{\sigma_{pt}}=\frac{9}{\alpha^2}\frac{\Gamma(Z\to e^+e^-)\Gamma(Z\to f\bar{f})}{[\Gamma(Z\to \text{all})]^2}, \tag{5.5}$$

with

$$\sigma_{pt}=\sigma(e^+e^-\to\mu^+\mu^-)=\frac{4\pi}{3}\frac{\alpha^2}{s}. \tag{5.6}$$

Of course, due to finite-energy resolution and radiative effects, this resonance cross section is not what is observed directly. However, the cross section integrated over the resonance region can be directly measured and is quite meaningful:

$$\int\sigma^{\mu\mu}dM=\frac{6\pi^2}{M_Z{}^2}\frac{\Gamma_{\mu\mu}{}^2}{\Gamma_{\text{tot}}}, \quad \text{etc.} \tag{5.7}$$

These intergrated cross sections allow an indirect measurement of the various branching ratios. To compare integrated cross sections for the two models we take ratios such as

$$R\equiv\frac{\int\sigma^{\mu\mu}_{L\times R}dM}{\int\sigma^{\mu\mu}_{WS}dM}=\left(\frac{M_{WS}}{M_{L\times R}}\right)^2\frac{(\Gamma B^2)_{L\times R}}{(\Gamma B^2)_{WS}}, \tag{5.8}$$

where the B's are the relevant branching ratios for the process being considered and Γ is the total width of the Z boson. The values for these parameters in the various models can be read off directly from Figs. 6–12 and so R is immediately calculable. Obviously, for Z_1 the ratio R is of order unity except in extreme cases; let us look at a particular case for Z_2 ($\epsilon=0$, $\zeta=0.85$, $\sin^2\theta=0.45$) for which

$$M_2\simeq 329\ \text{GeV},\quad B_{\mu\mu}\simeq 1.8\%,\qquad \Gamma\simeq 8.3\ \text{GeV}, \tag{5.9}$$

and thus

$$\int\sigma^{\mu\mu}dM\simeq 6.10^{-31}\ \text{cm}^2\,\text{MeV}. \tag{5.10}$$

With a luminosity of ~10^{32} and an energy resolution of ~30 MeV this yields an event rate[17] of ~10^4/day at LEP (assuming a sufficient center-of-mass energy). Detecting such a particle would not prove difficult even if the luminosity were lowered by a substantial factor; this rate is comparable (within an order of magnitude) to that found for the Z of the standard model. We conclude that LEP, with sufficient center-of-mass energy, could easily produce an observable heavy-Z resonance with sufficient counting rates.

It should be noted that the existence of a heavy Z can also be inferred from the behavior of the vari-

ous helicity and asymmetry parameters, introduced earlier, in the $\sqrt{s}$ region between the two Z's.

We believe that it may be possible to produce heavier Z's directly at ISABELLE with an appreciable counting rate for certain ranges of the model parameters if the backgrounds are sufficiently under control. LEP may provide indirect evidence for heavy-Z production even if its highest $\sqrt{s}$ value is below the heavy-Z mass. Finding the heavy Z (if it exists) or indirect evidence of its existence will prove the necessity of extending the weak-interaction gauge group.

VI. CONCLUSION

In this paper, we have made a comparison of the predictions for the high-Q^2 behavior of pp, $\bar{p}p$, and e^+e^- interactions of the Weinberg-Salam and left-right-symmetric $SU_L(2)\times SU_R(2)\times U(1)$ models. We have found that for the set of models allowed by the low-energy data [Eq. (2.6)], high-energy colliders may provide very discriminating tests. In e^+e^- collisions below the Z (or Z_1) mass, many models can be easily discriminated by measurements of various asymmetries at the 5–10% level. The actual production of the WS Z (or Z_1) boson at either LEP, ISABELLE, or CERN provides further constraints through its mass and values of its various branching ratios.

The most discriminating tests for models with weak gauge groups larger than $SU(2)\times U(1)$ is the discovery of a heavy ($\gtrsim$150 GeV) neutral gauge boson (Z_2) in addition to the usual light ($\simeq$90 GeV) gauge boson (Z or Z_1). With planned pp and $\bar{p}p$ colliders at BNL and CERN the possibility exists that this heavy Z may be produced with a sufficient rate to be detected. Given the wide range of allowed parameters for the left-right-symmetric model we have found that there do exist heavy Z's which can be produced at an appreciable rate (neglecting QCD corrections).

To complete the analysis presented here, we need to further constrain the region of allowed parameters. This will probably be done at PEP and PETRA and will allow us to make more concrete predictions about the properties of the heavier Z.

We conclude by stating that the most conclusive test at high Q^2 of the left-right-symmetric model may be found in the physics of high-energy colliders.

ACKNOWLEDGMENTS

The author would like to thank D. P. Sidhu, F. E. Paige, and T. L. Trueman for discussions related to this work. This research was performed under Contract No. EY-76-C-02-0016 with the U.S. Department of Energy.

[1]L. M. Sehgal, Phys. Lett. 71B, 99 (1977); G. Ecker, *ibid.* 72B, 450 (1978); P. Q. Hung and J. J. Sakurai, *ibid.* 72B, 208 (1978); L. F. Abbot and R. M. Barnett, Phys. Rev. Lett. 40, 1303 (1978); P. Langacker and D. P. Sidhu, Phys. Lett. 74B, 233 (1978); Phys. Rev. Lett. 41, 732 (1978).

[2]L. M. Barkov and M. S. Zolotorev, Zh. Eksp. Teor. Fiz. Pis'ma Red. 27, 379 (1978) [JETP Lett. 27, 357 (1978)].

[3]R. Conti *et al.*, Phys. Rev. Lett. 42, 343 (1979).

[4]C. Y. Prescott *et al.*, Phys. Lett. 77B, 347 (1978); 84B, 524 (1979).

[5]S. Weinberg, Phys. Rev. Lett. 19, 1364 (1967); Phys. Rev. D 5, 1412 (1972); A. Salam, in *Elementary Particle Theory: Relativistic Groups and Analyticity (Nobel Symposium No. 8)*, edited by N. Swartholm (Almqvist and Wiksell, Stockholm, 1968), p. 367; S. Glashow, J. Iliopoulos, and L. Maiani, Phys. Rev. D 2, 1285 (1970).

[6]D. P. Sidhu, BNL Report No. BNL-26192, 1979 (unpublished); D. P. Sidhu and T. N. Tudron, Phys. Rev. D 21, 45 (1980).

[7]T. G. Rizzo and D. P. Sidhu, Phys. Rev. D 21, 1209 (1980).

[8]See A. Roberts, Fermilab Report No. Fermilab-Conf-79/32-EXP, 1979 (unpublished), and references therein.

[9]CERN Yellow Report No. 78-02, 1978 (unpublished).

[10]L. Camilleri *et al.*, CERN Yellow Report 76-18, 1976 (unpublished).

[11]G. Senjanović, Nucl. Phys. B153, 334 (1979).

[12]A. De Rújula, H. Georgi, and S. Glashow, Phys. Rev. D 12, 147 (1975).

[13]S. D. Drell and T.-M. Yan, Phys. Rev. Lett. 25, 316 (1970); Ann. Phys. (N.Y.) 66, 578 (1971).

[14]C. Quigg, Rev. Mod. Phys. 49, 297 (1977); R. F. Peierls, T. L. Trueman, and L.-L. Wang, Phys. Rev. D 16, 1397 (1977).

[15]J. Kogut and J. Shigemitsu, Nucl. Phys. B129, 461 (1977).

[16]R. D. Field and R. P. Feynman, Phys. Rev. D 15, 2590 (1977).

[17]G. J. Tarnopolsky, Phys. Lett. 79B, 451 (1978).

[18]Proceedings of the 1977 Summer Workshop, edited by J. R. Sanford, BNL Report No. BNL-50721, 1977 (unpublished); Proceedings of the 1978 Summer Workshop, edited by J. R. Sanford, BNL Report No. BNL-50885, 1978 (unpublished).

[19]M. Jacob *et al.*, Proceedings of the LEP Summer Study, CERN Yellow Report No. 79-01, 1979 (unpublished), Vols. I and II.